The Astronomical Journal, 155:222 (9pp), 2018 May https://doi.org/10.3847/1538-3881/aabde8

Three Small Planets Transiting the Bright Young Field Star K2-233

Trevor J. David[1], Ian J. M. Crossfield[2], Björn Benneke[3], Erik A. Petigura[4,15], Erica J. Gonzales[5,16], Joshua E. Schlieder[6], Liang Yu[2], Howard T. Isaacson[7], Andrew W. Howard[4], David R. Ciardi[8], Eric E. Mamajek[1,9], Lynne A. Hillenbrand[4], Ann Marie Cody[10], Adric Riedel[11], Hans Martin Schwengeler[12], Christopher Tanner[13], and Martin Ende[14]

[1] Jet Propulsion Laboratory, California Institute of Technology, 4800 Oak Grove Drive, Pasadena, CA 91109, USA; trevor.j.david@jpl.nasa.gov
[2] Department of Physics, Massachusetts Institute of Technology, Cambridge, MA, USA
[3] Département de Physique, Université de Montréal, Montreal, H3T J4, Canada
[4] Department of Astronomy, California Institute of Technology, Pasadena, CA 91125, USA
[5] Astronomy and Astrophysics Department, University of California, Santa Cruz, CA, USA
[6] Exoplanets and Stellar Astrophysics Laboratory, Code 667, NASA Goddard Space Flight Center, Greenbelt, MD 20771, USA
[7] Astronomy Department, University of California, Berkeley, CA 94720, USA
[8] Caltech/IPAC-NASA Exoplanet Science Institute, Pasadena, CA 91125, USA
[9] Department of Physics & Astronomy, University of Rochester, Rochester, NY 14627, USA
[10] NASA Ames Research Center, Moffet Field, CA 94035, USA
[11] Space Telescope Science Institute, 3700 San Martin Drive, Baltimore, MD 21218, USA
[12] Planet Hunter, Bottmingen, Switzerland
[13] Exoplanet Explorers Volunteer, Thuringia, Germany
[14] Exoplanet Explorers Volunteer, Dresden, Germany
Received 2018 January 31; revised 2018 April 9; accepted 2018 April 10; published 2018 May 3

Abstract

We report the detection of three small transiting planets around the young K3 dwarf K2-233 (2MASS J15215519 −2013539) from observations during Campaign 15 of the *K2* mission. The star is relatively nearby ($d = 69$ pc) and bright ($V = 10.7$ mag, $K_s = 8.4$ mag), making the planetary system an attractive target for radial velocity follow-up and atmospheric characterization with the *James Webb Space Telescope*. The inner two planets are hot super-Earths ($R_b = 1.40 \pm 0.06\,R_\oplus$, $R_c = 1.34 \pm 0.08\,R_\oplus$), while the outer planet is a warm sub-Neptune ($R_d = 2.6 \pm 0.1\,R_\oplus$). We estimate the stellar age to be 360^{+490}_{-140} Myr based on rotation, activity, and kinematic indicators. The K2-233 system is particularly interesting given recent evidence for inflated radii in planets around similarly aged stars, a trend potentially related to photo-evaporation, core cooling, or both mechanisms.

Key words: planetary systems – planets and satellites: gaseous planets – planets and satellites: physical evolution – planets and satellites: terrestrial planets – stars: individual (EPIC 249622103)

1. Introduction

Kepler provided a large, relatively homogeneous sample from which the statistical frequencies of exoplanets have been robustly determined. Though the primary mission was to measure the prevalence of Earth-sized planets around solar-type stars (e.g., Petigura et al. 2013a), the data also provided a number of insights into planet formation outcomes more generally, such as the surprising abundance of sub-Neptunes, trends in planet occurrence with stellar mass (Howard et al. 2012), and fine structure in the size distribution of small planets (Fulton et al. 2017). Because the mission surveyed ∼1/400 of the sky, however, a typical *Kepler* planet host is relatively faint and presents challenges to characterization efforts like radial velocity mass measurements or transmission spectroscopy.

In contrast, the *K2* mission (Howell et al. 2014) to date has observed 15× the area of the prime *Kepler* mission, casting a wider net for planets around bright stars more evenly distributed on the sky. Statistical exoplanet studies within carefully defined sub-samples may yet prove fruitful but, like its predecessor, *K2* has already revealed a great number of surprises: a transiting minor planet around a stellar remnant (Vanderburg et al. 2015), the possible detection of accretion pulses driven by the orbital motion of an infant hot Jupiter (Biddle et al. 2018), and a chain of five near-resonant planets discovered by citizen scientists (Christiansen et al. 2018), to name a few.

Two domains probed by *K2*, which will form an important part of the mission's legacy, are transiting planet hosts that are bright and/or young. The mission has yielded all of the known transiting planets in young clusters and associations to date (see Rizzuto et al. 2017, for a review), as well as a number of planets around active field stars that are likely to be moderately young (e.g., Dai et al. 2017; Gaidos et al. 2017; Barragán et al. 2018). *K2* is also responsible for contributing some of the brightest known transiting planet hosts, such as HIP 41378 (Vanderburg et al. 2016a), HD 106315 (Crossfield et al. 2017; Rodriguez et al. 2017), HD 3167 (Vanderburg et al. 2016b; Gandolfi et al. 2017), and GJ 9827 (Niraula et al. 2017; Rodriguez et al. 2018). Until *TESS* extends the sample of bright transiting planet hosts, these systems remain some of the most amenable to atmospheric characterization via transit transmission spectroscopy. The properties of young planets are particularly interesting, given suggestions that larger sub-Neptunes are preferentially found around young stars (Berger et al. 2018) and that such planets may experience evaporative mass-loss at early stages (e.g., Lopez & Fortney 2013). Here, we report the discovery of three small transiting planets around a star that is both relatively bright and young. The system, K2-233, is an attractive target for both radial velocity work and atmospheric characterization.

[15] NASA Hubble Fellow.
[16] NSF Graduate Research Fellow.

2. *K2* Observations

K2-233 (also EPIC 249622103 and 2MASS J15215519 −2013539) was observed during Campaign 15 of the *K2* mission.[17] Following an approach similar to that of Christiansen et al. (2018), we analyzed the raw cadence pixel data released by the *K2* project by first converting the cadence data into target pixel files with `kadenza`[18] (Barentsen 2017). From there, we followed our team's standard discovery approach (see, e.g., Crossfield et al. 2016): we constructed a light curve from aperture photometry with `k2phot`,[19] which simultaneously models stellar variability and spacecraft systematics with a Gaussian process. From this light curve (Figure 1), we found three transit signals detected with the `terra`[20] program (Petigura et al. 2013a, 2013b). The transit signals were also independently discovered by citizen scientists as part of the Planet Hunters and Exoplanet Explorers projects.[21,22]

Prior to fitting transit models to the *K2* data, we removed the stellar variability via cubic basis spline fits with iterative outlier rejection. We used the rms in the flattened light curve as the flux uncertainty for each measurement. We then fit analytic transit models, generated with the `PyTransit`[23] package (Parviainen 2015), to the observations in order to determine the following free parameters: the orbital period P, time of mid-transit T_0, radius ratio R_P/R_*, scaled semimajor axis a/R_*, and cosine of the inclination $\cos i$. We first performed Levenberg–Marquardt (L–M) fits to find initial parameter estimates, then used the `emcee` affine invariant implementation of the Markov chain Monte Carlo (MCMC) method (Foreman-Mackey et al. 2013) to robustly determine the uncertainties on these parameters. The target probability density to be sampled in these simulations was

$$\ln \mathcal{L} = -\frac{1}{2}\chi^2 - \frac{1}{2}\frac{(\rho_* - \mu_{\rho_*})^2}{\sigma^2_{\rho_*}}, \quad (1)$$

where the first term is the likelihood and the second term describes a Gaussian prior on the mean stellar density, ρ_*, with $\mu_{\rho_*} = 2.73\ \mathrm{g\ cm^{-3}}$ and $\sigma_{\rho_*} = 0.31\ \mathrm{g\ cm^{-3}}$, based on our stellar characterization in Section 3. We used $\chi^2 = \sum(f_n - m_n)^2/\sigma_n^2$, where f_n and m_n are the nth flux observation and transit model values, respectively, and σ_n is the individual flux uncertainty. This assumes uncorrelated measurement uncertainties, which is not strictly true due to, e.g., short-term stellar variability and our procedure of removing the stellar variability prior to fitting. Additionally, we imposed uniform priors on the following parameters: P (centered on the initial estimate, with width 0.01 days), T_0 (centered on the initial estimate with width $0.06P$), R_P/R_* (from -1 to $+1$), a/R_* (from 1 to ∞), $\cos i$ (from $\cos 50^\circ$ to $\cos 90^\circ$). We assumed a quadratic limb-darkening law with coefficients $u_1 = 0.587$ and $u_2 = 0.136$, informed by our spectroscopic stellar characterization (Section 3) and the values tabulated by Claret & Bloemen (2011). The transit models were numerically integrated to match the *Kepler* long-cadence integration using a supersampling factor of 10.

We initialized the MCMC sampler with 40 walkers around the preliminary L–M solution. For each free parameter, the integrated autocorrelation time, $\hat{\tau}$, of the MCMC chain was calculated every 2000 steps. When the chain length exceeded $100 \times \hat{\tau}$ for all parameters and when these $\hat{\tau}$ estimates changed by less than 1%, the chain was considered to be converged and the MCMC procedure was halted. We estimated the burn-in as five times the maximum autocorrelation time estimate, and from the trimmed chains, we calculated the 15.87, 50, and 84.13 percentile values for each parameter.[24] These parameters and derivative physical quantities are reported in Table 1.

We additionally performed fits with the eccentricity e and periastron longitude ω as free parameters with uniform priors on each. As expected, the relatively shallow transits provide only weak constraints on eccentricity of $e < 0.53, 0.54, 0.45$ at 95% confidence for planets b, c, and d, respectively. Orbit crossing constraints would restrict the range of allowed eccentricities to even smaller values. We ultimately adopted the circular model because it is simpler (lower BIC); the other fitted parameters changed by $<1\sigma$, and previous studies of compact multi-planet systems find typical eccentricities of a few percent (Hadden & Lithwick 2014; Van Eylen & Albrecht 2015; Xie et al. 2016). We also investigated the effect of eliminating the Gaussian prior on the mean stellar density prior (requiring only that $a/R_* > 1$). These fits, which are presented in the Appendix, resulted in R_P/R_* distributions with longer tails toward more positive values, corresponding to solutions with higher impact parameters and unrealistically low stellar densities. The median parameter values from these fits all changed by $\lesssim 1\sigma$ and the stellar density implied by each planet was within 1σ of the value we adopted, providing assurance that the star has been properly characterized and our prior on this parameter is well-justified.

3. Stellar Characterization

We acquired high-resolution optical spectroscopy of K2-233 on UT 2018 January 22 (BJD 2458141.152490) with Keck I/HIRES (Vogt et al. 1994) using standard procedures of the California Planet Search (Howard et al. 2010). We then used SpecMatch (Petigura 2015) to compare the spectrum to Coelho et al. (2005) model atmospheres and determined $T_{\rm eff} = 4950 \pm 100$ K, $\log g = 4.71 \pm 0.10$ dex, [Fe/H] $= 0.07 \pm 0.06$ dex, and $v \sin i_* = 4.5 \pm 1.0\ \mathrm{km\ s^{-1}}$. As a consistency check, we also used SpecMatch-Emp (Yee et al. 2017) to compare the spectrum with a library of empirical spectra of benchmark stars, finding values for $T_{\rm eff}$, R_*, and [Fe/H] that are consistent within 1σ of those found with SpecMatch. From this analysis, we found the best-matching template spectrum to be that of HD 110463 (K3V), from which we assigned a spectral type of K3 to K2-233. A precise distance to K2-233 has been measured from trigonometric parallax (69 ± 1 pc; *Gaia* DR1), which provides tight constraints on the stellar parameters. With the `isoclassify` package (Huber et al. 2017), using the parallax, spectroscopic parameters ($T_{\rm eff}$, $\log g$, and [Fe/H]), and the 2MASS JHK$_s$ magnitudes as input, we determined

[17] The star was proposed by several K2 teams: GO15020 (PI Adams), GO15023 (PI Hillenbrand), GO15043 (PI Rizutto), and GO15052 (PI Stello).
[18] https://github.com/KeplerGO/kadenza
[19] https://github.com/petigura/k2phot
[20] https://github.com/petigura/terra
[21] https://www.planethunters.org/
[22] https://www.zooniverse.org/projects/ianc2/exoplanet-explorers
[23] https://github.com/hpparvi/PyTransit
[24] Transit fit posteriors are available at https://exofop.ipac.caltech.edu/k2/edit_target.php?id=249622103.

Table 1
Planet Parameters in the K2-233 System

Parameter	Planet b	Planet c	Planet d
Directly fitted parameters			
Time of mid-transit, T_0 (BJD-2450000)	$7991.6910^{+0.0026}_{-0.0025}$	$7996.3522^{+0.0056}_{-0.0057}$	$8005.5801^{+0.0025}_{-0.0024}$
Orbital period, P (days)	$2.46746^{+0.00014}_{-0.00014}$	$7.06142^{+0.00084}_{-0.00084}$	$24.3662^{+0.0021}_{-0.0021}$
Radius ratio, R_P/R_*	$0.01721^{+0.00049}_{-0.00047}$	$0.01643^{+0.00084}_{-0.00078}$	$0.03254^{+0.00080}_{-0.00079}$
Scaled semimajor axis, a/R_*	$9.49^{+0.29}_{-0.32}$	$19.34^{+0.67}_{-0.74}$	$44.2^{+1.6}_{-1.8}$
Cosine of inclination, $\cos i$	$0.021^{+0.016}_{-0.014}$	$0.0184^{+0.0082}_{-0.0107}$	$0.0113^{+0.0019}_{-0.0021}$
Derived parameters			
Planet radius, R_P ($R_\oplus$)	$1.398^{+0.062}_{-0.060}$	$1.335^{+0.083}_{-0.077}$	$2.64^{+0.11}_{-0.11}$
Inclination, i (deg)	$88.79^{+0.82}_{-0.94}$	$88.95^{+0.61}_{-0.47}$	$89.35^{+0.12}_{-0.11}$
Impact parameter, b	$0.20^{+0.15}_{-0.14}$	$0.36^{+0.15}_{-0.21}$	$0.500^{+0.065}_{-0.079}$
Total duration, T_{14} (hr)	$1.969^{+0.062}_{-0.063}$	$2.65^{+0.13}_{-0.15}$	$3.808^{+0.089}_{-0.088}$
Full duration, T_{23} (hr)	$1.899^{+0.062}_{-0.065}$	$2.55^{+0.14}_{-0.17}$	$3.49^{+0.10}_{-0.10}$
Semimajor axis, a (au)	$0.03317^{+0.00044}_{-0.00045}$	$0.06687^{+0.00088}_{-0.00090}$	$0.1527^{+0.0020}_{-0.0021}$
Insolation flux, S ($S_\oplus$)	273^{+30}_{-30}	$67.1^{+7.4}_{-7.3}$	$12.9^{+1.4}_{-1.4}$
Equilibrium temperature, $T_{\rm eq}$ (K)[a]	1040^{+28}_{-26}	728^{+20}_{-19}	482^{+14}_{-13}

Note. Reported values and 1σ errors are the 50, 15.87, and 84.13 percentile levels from the MCMC chain. The fit presented here assumed $e = 0$, a Gaussian prior on the mean stellar density ($\mu_{\rho_*} = 2.73$ g cm^{-3}, $\sigma_{\rho_*} = 0.31$ g cm^{-3}), quadratic limb-darkening coefficients $u_1 = 0.587$, $u_2 = 0.136$, and no contaminating flux. Derived parameters assume all three planets are orbiting the target star, and that the target star is single.
[a] Assuming an albedo of 0.3.

precise values for the model-dependent mass, $M_* = 0.80 \pm 0.02\ M_\odot$, and radius, $R_* = 0.745 \pm 0.011\ R_\odot$. To account for possible systematic uncertainties in the models, we added in quadrature a 2% uncertainty in these parameters. Combined with our spectroscopic $T_{\rm eff}$, the stellar radius and Stefan–Boltzmann law imply a luminosity of $L_* = 0.300 \pm 0.032\ L_\odot$.

In an effort to better constrain the age of the system, we next considered the stellar kinematics, rotation, activity, and spectroscopic age indicators. The barycentric radial velocity was measured to be -9.73 ± 0.20 km s^{-1} using the telluric A and B absorption bands as a wavelength reference (Chubak et al. 2012). Combined with the proper motions and distance from *Gaia*, we found the stellar kinematics are not a good match to any known moving groups, nearby open clusters, or star-forming regions. Using the BANYAN Σ tool (Gagné et al. 2018), we found a 68.5% probability that the star belongs to the field population, with the remaining 31.5% probability assigned to membership in the Upper Scorpius OB association. The mean distance to Upper Scorpius is ∼140 pc, with a unidirectional spread of ≲35 pc. Given the precisely determined distance (at half the mean distance to Upper Scorpius), a radius and mean stellar density consistent with a main sequence star, and lack of lithium absorption (discussed below), we can confidently rule out that K2-233 belongs to that association. Based on age diagnostics from the stellar rotation and activity, we suggest K2-233 is a young field star.

From an autocorrelation function (ACF) analysis of the light curve, we measured a rotation period of $P_{\rm rot} = 9.754 \pm 0.038$ days. The period was determined by the slope of a linear fit to the first four peaks of the ACF plus the origin, and the uncertainty was estimated from the scatter about that fit. We note that typical observed rates of surface differential rotation (≲0.07 rad days^{-1}) in dwarf stars of a similar temperature and rotation period might introduce an additional uncertainty in the rotation period of ≲1.4 days. In period–color space (Figure 2), the star is situated between members of the Pleiades (∼125 Myr) and Praesepe (∼790 Myr), suggesting an age intermediate to these clusters if the star is on the main sequence (Rebull et al. 2016, 2017). The variability amplitude, 0.014 mag (measured from the 10th to the 90th percentile) is also similar to those seen among Pleiades and Praesepe members of a similar color (Rebull et al. 2016, 2017). Different gyrochronology relations predict ages of 270^{+80}_{-70} Myr (Barnes 2007), 440^{+120}_{-110} Myr (Mamajek & Hillenbrand 2008), and 500^{+140}_{-120} Myr (Angus et al. 2015), where these estimates reflect the 16th, 50th, and 84th percentile values adopting a conservative error on the rotation period of 1.4 days to allow for the possibility of differential rotation. Existing gyrochronology relations are in need of re-calibration, so these ages should be regarded with caution, but all relations suggest an age younger than 1 Gyr.

The HIRES spectrum shows Hα in absorption and no detectable absorption at Li I 6708 Å, which argues for an age older than that of the Pleiades. From the spectrum, we also measured the $S_{\rm HK}$ index and $\log R'_{\rm HK} = -4.361$ dex using the method of Isaacson & Fischer (2010), which is a value typical for Hyades (∼625–850 Myr) and the Ursa Major moving group (∼400–600 Myr) members of a similar color (see Figures 4 and 5 of Mamajek & Hillenbrand 2008). From the Mamajek & Hillenbrand (2008) activity–age relation, we calculated an age of 220 Myr, consistent with the younger gyrochronology age quoted above. The age relations considered are here are statistical in nature and carry large uncertainties. New calibrations of age–activity and gyrochronology relations are clearly in order, but outside of the scope of this paper. We ultimately adopt an age of $\tau_* \approx 360^{+490}_{-140}$ Myr, corresponding to the mean of the four estimates above, with the lower bound originating from the activity age and the upper bound from the oldest ages suggested for the Hyades and Praesepe clusters. We

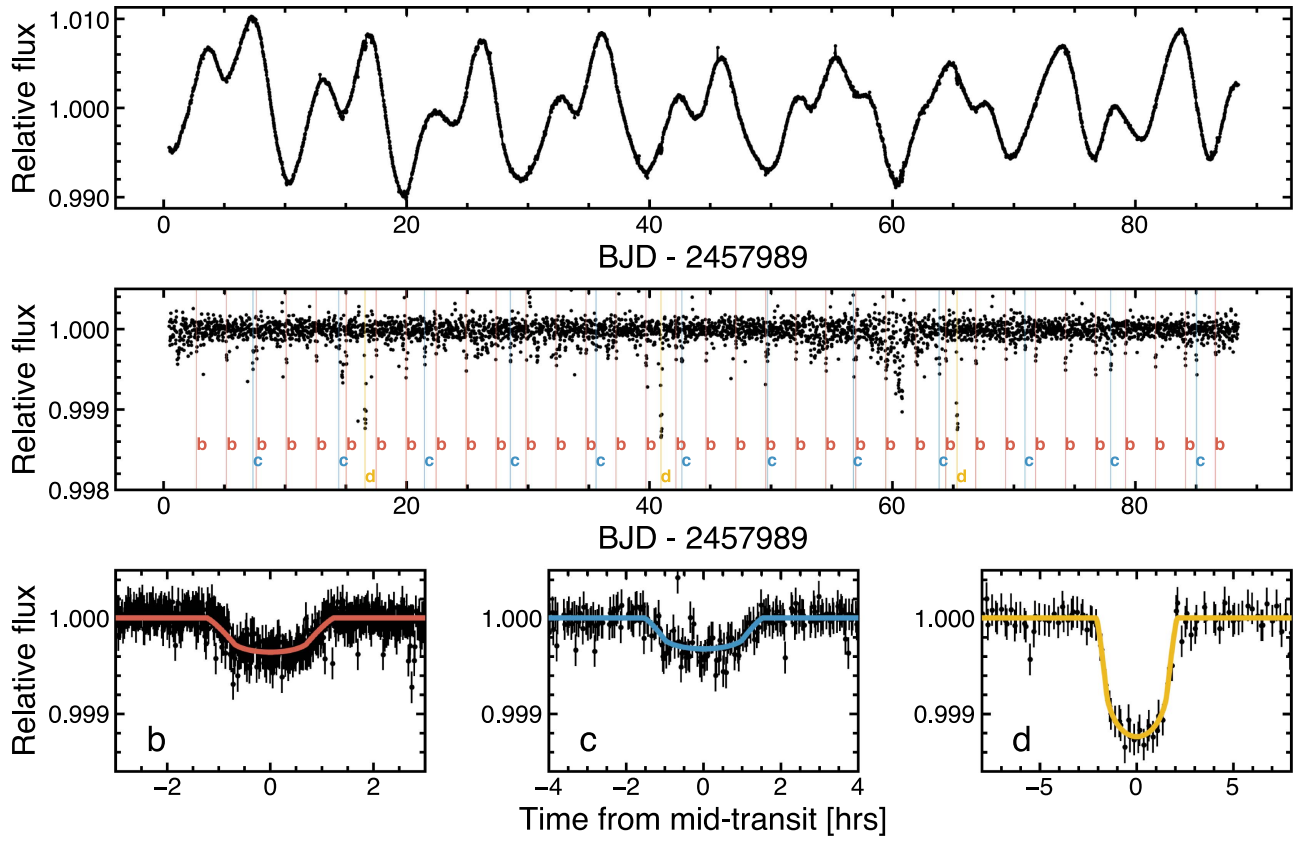

Figure 1. Full *K2* light curve of K2-233 (top), with the stellar variability removed and individual transits shown (middle), and phase-folded to the transits of planets b, c, and d with transit model fits shown as shaded lines (bottom).

summarize the basic observables and results of our stellar characterization analyses in Table 2.

4. Validating the Planets

The *K2* photometry were extracted from a rectangular aperture $24'' \times 36''$ in size. Pan-STARRS1 imaging shows there are no stars of comparable brightness within 1 arcminute, excluding the possibility that the transit signals arise from a widely separated companion. We acquired high spatial resolution imaging in the Br-γ band with Keck II/NIRC2 on UT 2017 December 29 and found no evidence for additional closely projected sources. Our 5σ contrast limits rule out sources with $\Delta\mathrm{mag} < 4$ outside of $0\farcs15$ and $\Delta\mathrm{mag} < 8$ from $1\farcs7$ to $3\farcs8$. Using the `vespa` package (Morton 2015), we statistically validated each planet, using $3\times$ the light curve rms as a conservative estimate of the maximum secondary eclipse depth and $0\farcs1$ ($3\times$ the NIRC2 resolution) as the photometric exclusion radius. From this analysis, we found false positive probabilities of 1.9×10^{-7}, 9.6×10^{-5}, and 6.9×10^{-7} for planets b, c, and d, respectively. Notably, these probabilities are calculated for each planet individually, and the overall false positive probability is in fact lower given the presence of multiple transiting planets.

We searched for secondary spectral lines in the HIRES spectrum using the method described in Kolbl et al. (2015) and found no evidence for a projected companion within $0\farcs8$ down to 3% the brightness of the primary star. We note this method is blind to companions with velocity separations <15 km s^{-1}. Further assurance that the transit signals originate from K2-233 comes from the transit fits with no direct prior on the mean stellar density. For each planet, the median value for the stellar density was within 1σ of the value we adopted for K2-233. While not conclusive, this observation is suggestive that the transiting planets are indeed orbiting K2-233. If K2-233 is a binary that evaded our detection, the planetary radii might be larger by $\lesssim$20%, given our vetting through high-resolution imaging and spectroscopy (Ciardi et al. 2015).

5. Discussion

Recent studies of *Kepler* multi-planet systems have found a high degree of intra-system uniformity (Ciardi et al. 2013; Fabrycky et al. 2014; Millholland et al. 2017). For example, planet sizes within an individual system are correlated, i.e., a planet is more likely to have a size similar to its neighbor than a size drawn at random from the observed distribution of planet sizes (Weiss et al. 2018, hereafter W18). The W18 study also found that (1) in about 65% of planet pairs in multi-transiting systems, the outer planet is larger than the inner planet, (2) planet separations are evenly spaced in log semimajor axis, and (3) adjacent planets tend to be separated by about 20 mutual Hill radii.

The K2-233 system largely adheres to these trends. The inner two planets have very similar sizes, while the outer planet is nearly twice as large as the inner two. This type of configuration is well within the scatter of Figure 2 from W18. The spacing between the three planets in log semimajor axis is indeed similar, about 0.307 dex and 0.358 dex (the planets

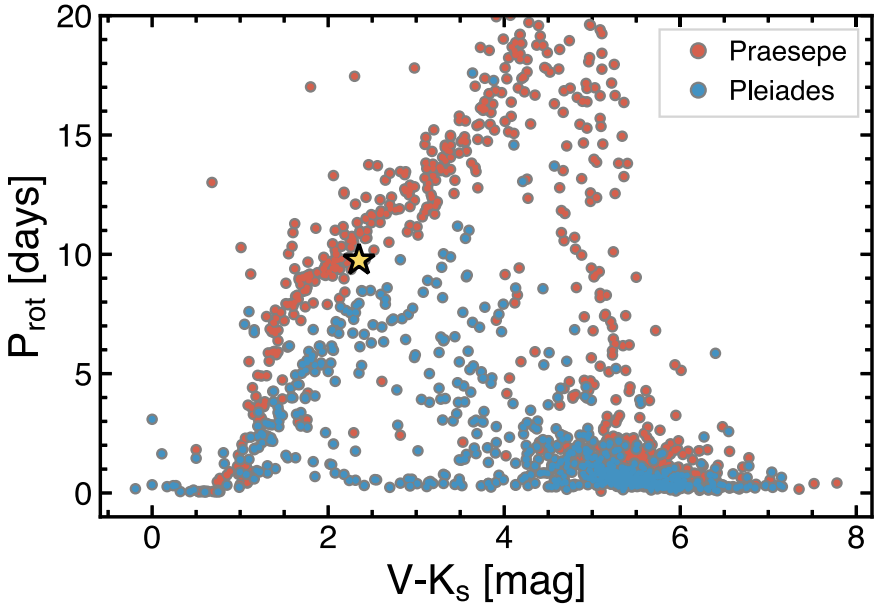

Figure 2. Period–color diagram for open cluster members observed by *K2* (Rebull et al. 2016, 2017) and K2-233 (gold star).

Table 2
Parameters of K2-233

Parameter	Value	Source
Kinematics and position		
R.A., J2000 (hh mm ss)	15 21 55.198	A
decl., J2000 (dd mm ss)	−20 13 53.991	A
Parallax (mas)	14.50 ± 0.23	A
Distance (pc)	69 ± 1	A
μ_α (mas yr^{-1})	−20.174 ± 0.687	A
μ_δ (mas yr^{-1})	−30.921 ± 0.412	A
Barycentric RV (km s^{-1})	−9.73 ± 0.20	B
Photometry		
G (mag)	10.333 ± 0.001	A
B (mag)	11.664 ± 0.027	C
V (mag)	10.726 ± 0.019	C
J (mag)	8.968 ± 0.020	D
H (mag)	8.501 ± 0.026	D
K_s (mag)	8.375 ± 0.023	D
Physical properties		
Spectral type	K3	B
$T_{\rm spec}$ (K)	4950 ± 100	B
M_* ($M_\odot$)	0.800 ± 0.032	B
R_* ($R_\odot$)	0.745 ± 0.025	B
L_* ($L_\odot$)	0.300 ± 0.032	B
log g (dex)	4.71 ± 0.10	B
[Fe/H] (dex)	0.07 ± 0.06	B
$v \sin i_*$ (km s^{-1})	4.5 ± 1.0	B
$P_{\rm rot}$ (days)	9.754 ± 0.038	B
$S_{\rm HK}$	0.686	B
log $R'_{\rm HK}$ (dex)	−4.36	B
τ_* (Myr)	360^{+490}_{-140}	B

Note. A: *Gaia* DR1, B: this work, C: APASS DR9, D: 2MASS.

are also apparently not in resonance, with period ratios of $P_c/P_b = 2.8618$ and $P_d/P_c = 3.4506$). Using the mass–radius relations of Wolfgang et al. (2016) and Chen & Kipping (2017) to predict planet masses based on the radii, we found $M_b \sim 2$–$5\ M_\oplus$, $M_c \sim 2$–$5\ M_\oplus$, and $M_d \sim 4$–$13\ M_\oplus$. From these predicted planet masses, the stellar mass, and orbital period ratios, we calculated that the planets in the K2-233 system are each separated by about 30–35 mutual Hill radii, a separation larger than ∼80% of adjacent pairs in three-planet systems. Observational biases are also important to consider, in that more compact systems are more likely to present multiple transiting planets. There may also be additional planets in the system that are non-transiting or below the sensitivity limits of the *K2* photometry. We also note that the W18 sample does not include stars with spectral types later than K3, though we do not expect this to dramatically change any of the conclusions presented here.

K2-233 is relatively bright and thus amenable to follow-up observations to characterize the planets in more detail. There are presently 18 (30) stars brighter than $V = 11$ mag ($K_s = 9$ mag) that host at least one known transiting planet smaller than 3 $R_\oplus$, and only 9 (13) of which host multiple transiting planets (Akeson et al. 2013).[25] Most of the bright multi-planet systems have been found with *K2*, but this will soon change with *TESS*. Based on the planetary radii and our current understanding of the exoplanet mass–radius relation, the inner two planets are likely to be rocky while the outer planet is likely to have a substantial volatile envelope (e.g., Fulton et al. 2017). From the planet mass estimates above, we calculated predicted radial velocity semi-amplitudes of ∼1.1–2.7, 0.8–1.9, and 1–3.3 m s^{-1} for planets b, c, and d, respectively. These amplitudes are at the limit of detectability for current instruments.

The apparent brightness and the relative small radius of the host star, K2-233, make all three planets potential targets for spectroscopic characterizations of their atmospheres. Depending on the surface gravity and hydrogen fraction of the atmosphere, the atmospheres of all three planets may be readily detectable using a single *JWST* visit. We estimate transit depth variation of the order of 10–100 ppm for

[25] https://exoplanetarchive.ipac.caltech.edu

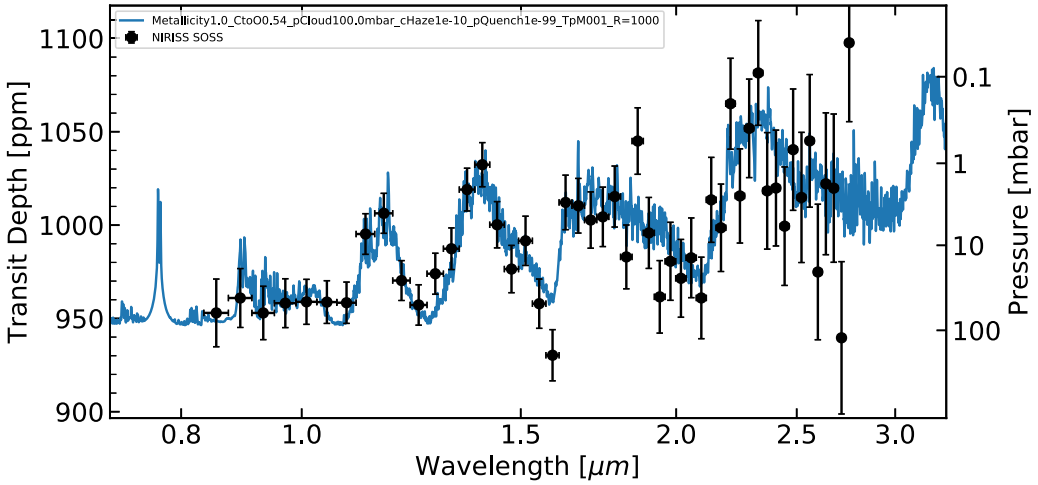

Figure 3. Model transmission spectra and simulated observations of the sub-Neptune K2-233 d, binned over 40 resolution elements resulting in $\lambda/\Delta\lambda = 150$–250. Assuming a planetary mass of 8 $M_{\oplus}$ and a single transit observation by *JWST/NIRISS*, water absorption is detectable at high significance for a H_2-dominated scenario with clouds below the 100 mbar level. Models were generated as described in Benneke & Seager (2012) and Benneke (2015). The observational uncertainties are 110% of the photon-noise limit accounting for the exact throughput, duty-cycle, and dispersion of the instruments.

atmospheres dominated by ices or hydrogen/helium, respectively. Figure 3 shows a simulated *JWST/NIRISS* transmission spectrum for the sub-Neptune K2-233 d assuming a planetary mass of 8 $M_{\oplus}$ and hydrogen-dominated atmosphere with clouds below the 100 mbar level. Transit depth variations as a function of wavelength, predominantly due to water vapor absorption, can readily be detected.

An interesting question worthy of further exploration is to what degree do the properties and configurations of exoplanetary systems vary in time? Berger et al. (2018) recently showed that larger sub-Neptunes preferentially orbit stars younger than the Hyades age (∼625–850 Myr). Such a trend might be the result of photo-evaporation, core cooling, or both. While K2-233 is merely a single planetary system, it joins a growing sample of young exoplanet hosts from which temporal trends in planet properties can be investigated.

This research was carried out at the Jet Propulsion Laboratory, California Institute of Technology, under a contract with the National Aeronautics and Space Administration. We thank Laura Kreidberg, Lauren Weiss, Dan Foreman-Mackey, and John Livingston for helpful discussions and the anonymous referee for comments which improved this manuscript. T.J.D. and E.E.M. gratefully acknowledge support from the Jet Propulsion Laboratory Exoplanetary Science Initiative. E.E.M. acknowledges support from the NASA NExSS program. This paper includes data collected by the *Kepler* mission. Funding for the *Kepler* mission is provided by the NASA Science Mission directorate. A portion of this work was supported by a NASA Keck PI Data Award, administered by the NASA Exoplanet Science Institute. Data presented herein were obtained at the W. M. Keck Observatory from telescope time allocated to the National Aeronautics and Space Administration through the agency's scientific partnership with the California Institute of Technology and the University of California. The Observatory was made possible by the generous financial support of the W. M. Keck Foundation. The authors wish to recognize and acknowledge the very significant cultural role and reverence that the summit of Maunakea has always had within the indigenous Hawaiian community. We are most fortunate to have the opportunity to conduct observations from this mountain.

Appendix

As mentioned in Section 2, we performed additional transit fits for each planet with no direct prior on the mean stellar density (requiring only $a/R_* > 1$ and assuming the same uniform prior on orbital period). We present the results of these fits in Table 3 and illustrate the parameter covariances from both fits in Figures 4, 5, and 6.

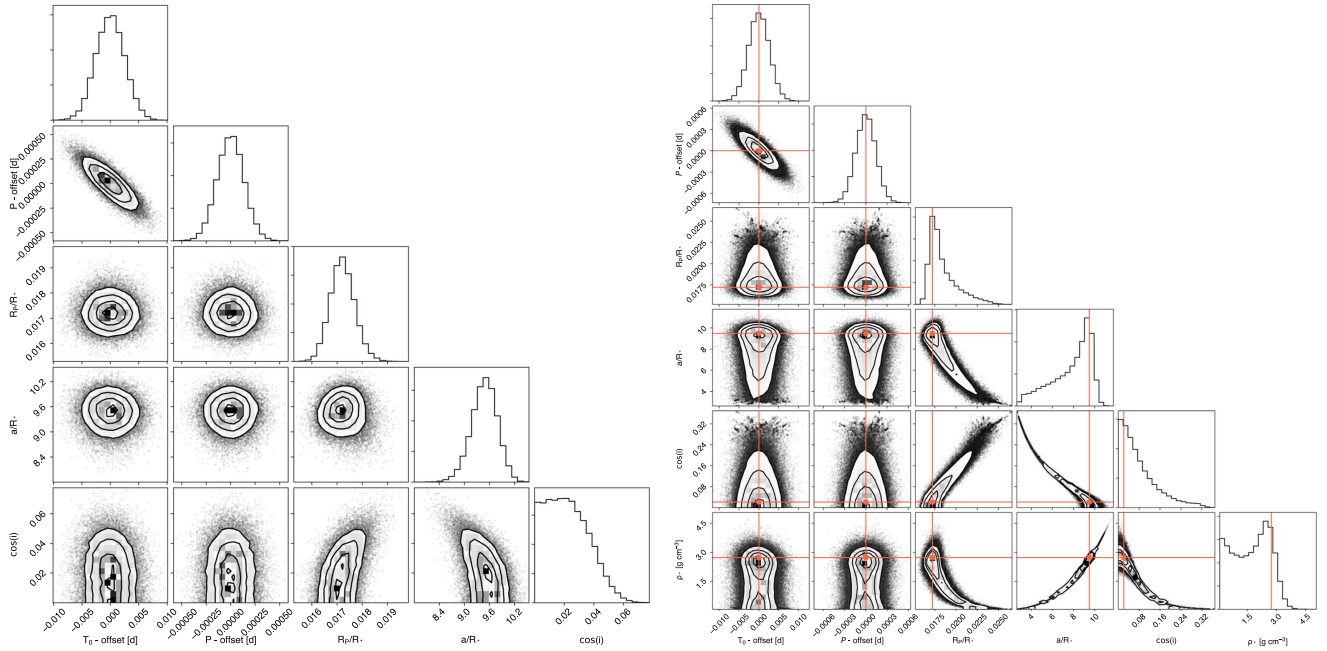

Figure 4. Corner plots from the planet b MCMC posterior samples in the case of a circular orbit with a Gaussian prior on mean stellar density (left) and with no direct prior on mean stellar density (right). At right, the positions of the red squares indicate the median values obtained (or assumed) from the fit with the imposed prior on mean stellar density.

Table 3
Planet Transit Fit Parameters with No Direct Prior on Mean Stellar Density

Parameter	Planet b	Planet c	Planet d
Directly fitted parameters			
Time of mid-transit, T_0 (BJD-2450000)	$7991.6911^{+0.0026}_{-0.0026}$	$7996.3522^{+0.0057}_{-0.0057}$	$8005.5801^{+0.0025}_{-0.0025}$
Orbital period, P (days)	$2.46746^{+0.00014}_{-0.00014}$	$7.06142^{+0.00083}_{-0.00083}$	$24.3662^{+0.0021}_{-0.0022}$
Radius ratio, R_P/R_*	$0.01789^{+0.00224}_{-0.00087}$	$0.0170^{+0.0021}_{-0.0010}$	$0.0325^{+0.0035}_{-0.0013}$
Scaled semimajor axis, a/R_*	$8.3^{+1.2}_{-2.8}$	$18.1^{+2.9}_{-6.1}$	$44.7^{+5.6}_{-13.2}$
Cosine of inclination, $\cos i$	$0.061^{+0.088}_{-0.044}$	$0.027^{+0.041}_{-0.020}$	$0.0108^{+0.0143}_{-0.0077}$
Derived parameters			
Planet radius, R_P ($R_\oplus$)	$1.462^{+0.180}_{-0.092}$	$1.39^{+0.17}_{-0.10}$	$2.66^{+0.28}_{-0.15}$
Inclination, i (deg)	$86.5^{+2.5}_{-5.1}$	$88.4^{+1.1}_{-2.4}$	$89.38^{+0.44}_{-0.82}$
Impact parameter, b	$0.51^{+0.32}_{-0.34}$	$0.50^{+0.32}_{-0.34}$	$0.48^{+0.31}_{-0.33}$
Total duration, T_{14} (hr)	$2.01^{+0.10}_{-0.09}$	$2.63^{+0.19}_{-0.17}$	$3.82^{+0.16}_{-0.11}$
Full duration, T_{23} (hr)	$1.873^{+0.092}_{-0.118}$	$2.45^{+0.18}_{-0.20}$	$3.45^{+0.12}_{-0.23}$
Semimajor axis, a (au)	$0.03317^{+0.00044}_{-0.00045}$	$0.06687^{+0.00088}_{-0.00090}$	$0.1527^{+0.0020}_{-0.0021}$
Insolation flux, S ($S_\oplus$)	273^{+30}_{-30}	$67.1^{+7.4}_{-7.3}$	$12.9^{+1.4}_{-1.4}$
Equilibrium temperature, $T_{\rm eq}$ (K)[a]	1110^{+248}_{-77}	753^{+172}_{-57}	480^{+91}_{-29}
Mean stellar density, ρ_* (g cm^{-3})	$1.81^{+0.90}_{-1.27}$	$2.3^{+1.3}_{-1.6}$	$2.9^{+1.2}_{-1.9}$

Note. In this fit, a circular orbit was assumed ($e = 0$), with no direct prior on the mean stellar density (only the requirement that $a/R_* > 1$). Reported values and 1σ errors are the 50, 15.87, and 84.13 percentile levels from the MCMC chain. The fits presented here assumed no contaminating flux and quadratic limb-darkening coefficients $u_1 = 0.587$, $u_2 = 0.136$. Derived parameters assume all three planets are orbiting the target star and that the target star is single.
[a] Assuming an albedo of 0.3.

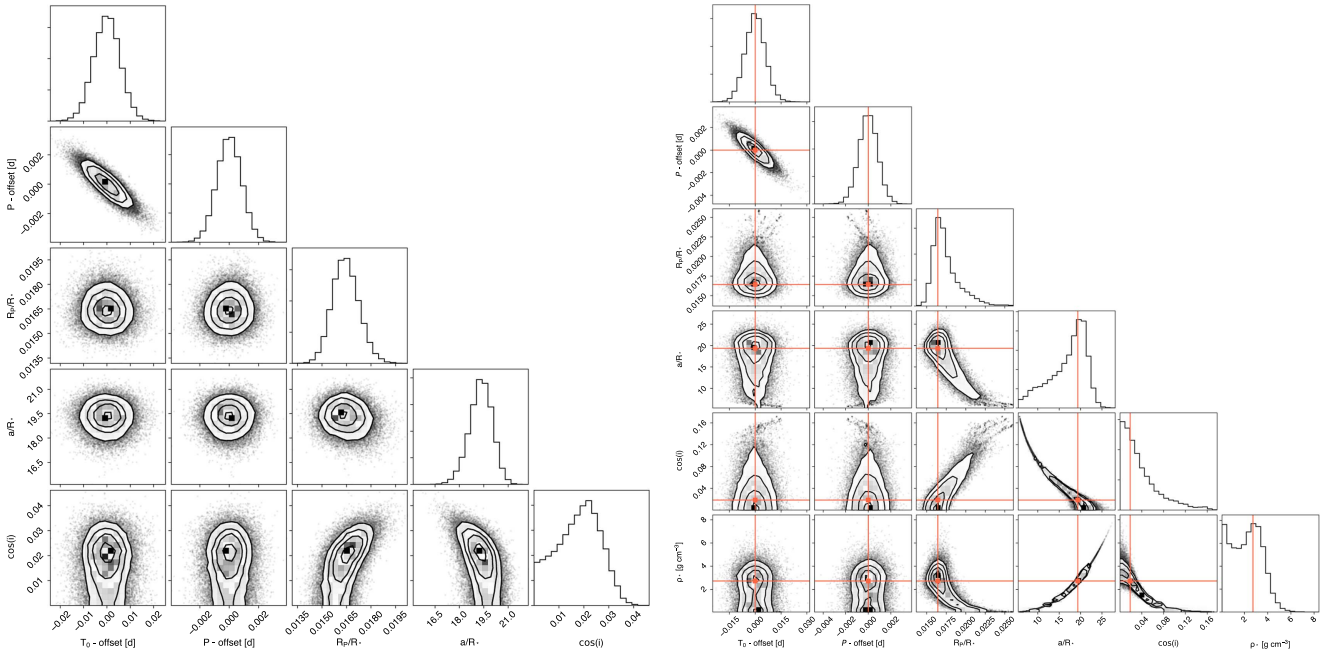

Figure 5. Same as Figure 4 for planet c.

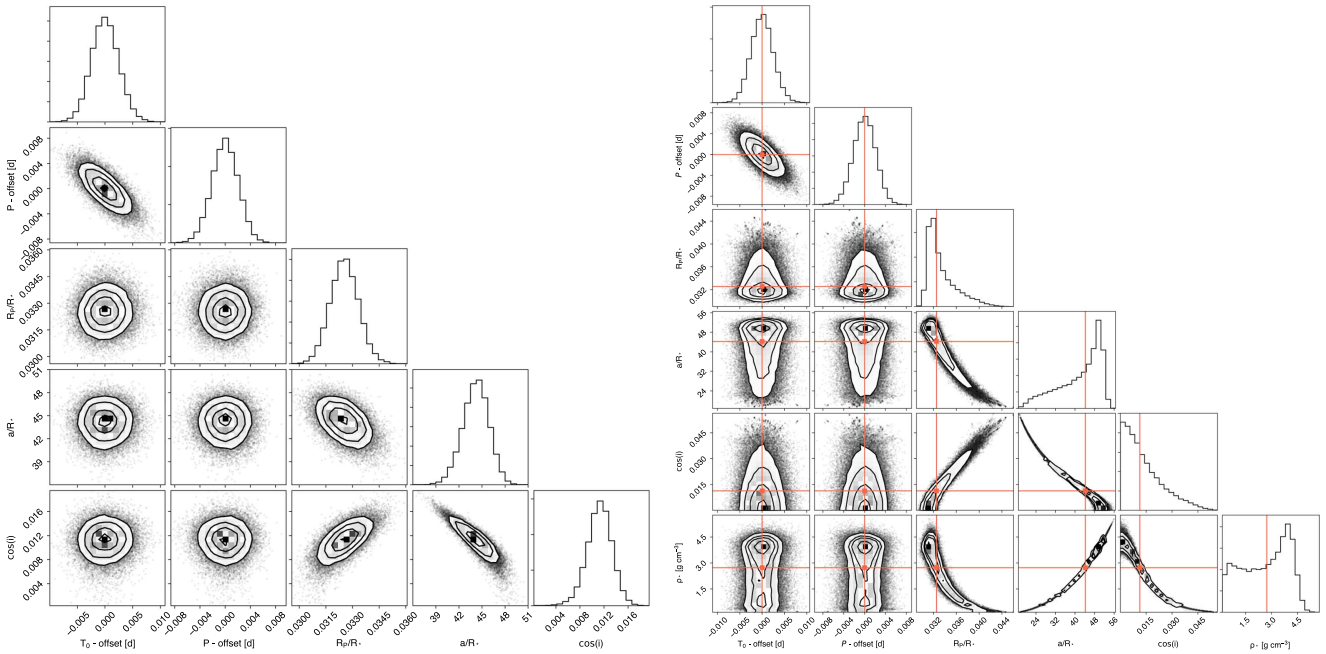

Figure 6. Same as Figure 4 for planet d.

ORCID iDs

Trevor J. David https://orcid.org/0000-0001-6534-6246
Ian J. M. Crossfield https://orcid.org/0000-0002-1835-1891
Björn Benneke https://orcid.org/0000-0001-5578-1498
Erik A. Petigura https://orcid.org/0000-0003-0967-2893
Joshua E. Schlieder https://orcid.org/0000-0001-5347-7062
Liang Yu https://orcid.org/0000-0003-1667-5427
Howard T. Isaacson https://orcid.org/0000-0002-0531-1073
Andrew W. Howard https://orcid.org/0000-0001-8638-0320
David R. Ciardi https://orcid.org/0000-0002-5741-3047
Eric E. Mamajek https://orcid.org/0000-0003-2008-1488
Ann Marie Cody https://orcid.org/0000-0002-3656-6706
Adric Riedel https://orcid.org/0000-0003-1645-8596

References

Akeson, R. L., Chen, X., Ciardi, D., et al. 2013, PASP, 125, 989
Angus, R., Aigrain, S., Foreman-Mackey, D., & McQuillan, A. 2015, MNRAS, 450, 1787
Barentsen, G. 2017, KeplerGO/kadenza, v2.0.2, Zenodo, doi:10.5281/zenodo.344973
Barnes, S. A. 2007, ApJ, 669, 1167
Barragán, O., Gandolfi, D., Smith, A. M. S., et al. 2018, MNRAS, 475, 1765
Benneke, B. 2015, arXiv:1504.07655
Benneke, B., & Seager, S. 2012, ApJ, 753, 100

Berger, T. A., Howard, A. W., & Boesgaard, A. M. 2018, ApJ, 855, 115
Biddle, L. I., Johns-Krull, C. M., Llama, J., Prato, L., & Skiff, B. A. 2018, ApJL, 853, L34
Chen, J., & Kipping, D. 2017, ApJ, 834, 17
Christiansen, J. L., Crossfield, I. J. M., Barentsen, G., et al. 2018, AJ, 155, 57
Chubak, C., Marcy, G., Fischer, D. A., et al. 2012, arXiv:1207.6212
Ciardi, D. R., Beichman, C. A., Horch, E. P., & Howell, S. B. 2015, ApJ, 805, 16
Ciardi, D. R., Fabrycky, D. C., Ford, E. B., et al. 2013, ApJ, 763, 41
Claret, A., & Bloemen, S. 2011, A&A, 529, A75
Coelho, P., Barbuy, B., Meléndez, J., Schiavon, R. P., & Castilho, B. V. 2005, A&A, 443, 735
Crossfield, I. J. M., Ciardi, D. R., Isaacson, H., et al. 2017, AJ, 153, 255
Crossfield, I. J. M., Ciardi, D. R., Petigura, E. A., et al. 2016, ApJS, 226, 7
Dai, F., Winn, J. N., Gandolfi, D., et al. 2017, AJ, 154, 226
Fabrycky, D. C., Lissauer, J. J., Ragozzine, D., et al. 2014, ApJ, 790, 146
Foreman-Mackey, D., Hogg, D. W., Lang, D., & Goodman, J. 2013, PASP, 125, 306
Fulton, B. J., Petigura, E. A., Howard, A. W., et al. 2017, AJ, 154, 109
Gagné, J., Mamajek, E. E., Malo, L., et al. 2018, ApJ, 856, 23
Gaidos, E., Mann, A. W., Rizzuto, A., et al. 2017, MNRAS, 464, 850
Gandolfi, D., Barragán, O., Hatzes, A. P., et al. 2017, AJ, 154, 123
Hadden, S., & Lithwick, Y. 2014, ApJ, 787, 80
Howard, A. W., Johnson, J. A., Marcy, G. W., et al. 2010, ApJ, 721, 1467
Howard, A. W., Marcy, G. W., Bryson, S. T., et al. 2012, ApJS, 201, 15
Howell, S. B., Sobeck, C., Haas, M., et al. 2014, PASP, 126, 398
Huber, D., Zinn, J., Bojsen-Hansen, M., et al. 2017, ApJ, 844, 102
Isaacson, H., & Fischer, D. 2010, ApJ, 725, 875
Kolbl, R., Marcy, G. W., Isaacson, H., & Howard, A. W. 2015, AJ, 149, 18
Lopez, E. D., & Fortney, J. J. 2013, ApJ, 776, 2
Mamajek, E. E., & Hillenbrand, L. A. 2008, ApJ, 687, 1264
Millholland, S., Wang, S., & Laughlin, G. 2017, ApJL, 849, L33
Morton, T. D. 2015, VESPA: False Positive Probabilities Calculator, Astrophysics Source Code Library, ascl:1503.011
Niraula, P., Redfield, S., Dai, F., et al. 2017, AJ, 154, 266
Parviainen, H. 2015, MNRAS, 450, 3233
Petigura, E. A. 2015, PhD thesis, Univ. California, Berkeley
Petigura, E. A., Howard, A. W., & Marcy, G. W. 2013a, PNAS, 110, 19273
Petigura, E. A., Marcy, G. W., & Howard, A. W. 2013b, ApJ, 770, 69
Rebull, L. M., Stauffer, J. R., Bouvier, J., et al. 2016, AJ, 152, 113
Rebull, L. M., Stauffer, J. R., Hillenbrand, L. A., et al. 2017, ApJ, 839, 92
Rizzuto, A. C., Mann, A. W., Vanderburg, A., Kraus, A. L., & Covey, K. R. 2017, AJ, 154, 224
Rodriguez, J. E., Vanderburg, A., Eastman, J. D., et al. 2018, AJ, 155, 72
Rodriguez, J. E., Zhou, G., Vanderburg, A., et al. 2017, AJ, 153, 256
Van Eylen, V., & Albrecht, S. 2015, ApJ, 808, 126
Vanderburg, A., Becker, J. C., Kristiansen, M. H., et al. 2016a, ApJL, 827, L10
Vanderburg, A., Bieryla, A., Duev, D. A., et al. 2016b, ApJL, 829, L9
Vanderburg, A., Johnson, J. A., Rappaport, S., et al. 2015, Natur, 526, 546
Vogt, S. S., Allen, S. L., Bigelow, B. C., et al. 1994, Proc. SPIE, 2198, 362
Weiss, L. M., Marcy, G. W., Petigura, E. A., et al. 2018, AJ, 155, 48
Wolfgang, A., Rogers, L. A., & Ford, E. B. 2016, ApJ, 825, 19
Xie, J.-W., Dong, S., Zhu, Z., et al. 2016, PNAS, 113, 11431
Yee, S. W., Petigura, E. A., & von Braun, K. 2017, ApJ, 836, 77